Local strain matching between Nb nanowires and a phase transforming NiTi matrix in an in-situ composite

Zhenyang Liu[a], Yinong Liu[b], Daqiang Jiang[a], Feng Yang[a], Shijie Hao[a], Yang Ren[c], Lishan Cui[a]*

a Department of Materials Science and Engineering, China University of Petroleum-Beijing, Beijing 102249, China
b School of Mechanical and Chemical Engineering, The University of Western Australia, Crawley, WA6009, Australia
c X-ray Science Division, Argon National Laboratory, Argonne, IL60439, USA

Abstract:
This study investigated the deformation behavior of Nb nanowires in composite, which consisting of a phase transforming NiTi matrix and presents a unique metallurgical system in terms of load transfer and strain coupling between two components. It is found that embedded Nb nanowires experienced compressive residual stress after an initial tensile deformation, implying the occurrence of internal plastic deformation on nanowires. This is attributed to the discrete strain field of NiTi matrix which deforms via first order stress-induced martensitic transformation.

Keywords：composite, NiTi shape memory alloy, nanowire, deformation behavior

Introduction

It is known that metallic nanowires exhibit exceptional mechanical properties far beyond the limitations of bulk materials, such as high strengths and high elastic strains [1, 2], largely due to the limited population or the total elimination of crystalline structural defects**.** Given this, it has been a keen material design strategy to incorporate metallic nanowires in metal matrices to create composites of superior mechanical performances. Several nanowire-metal systems have been tried, such as carbon nanotube and nanofiber reinforced metal matrix composites [3, 4], metal nitride-metal matrix composite [5] and multi-scale nanofilamentary composites [6-8]. Whereas achieving good improvements in mechanical properties, these composites have not yet delivered what may be expected of the exceptional properties of the nanowires based on the law of mixture. The main reason is that the embedded nanowires are normally found to exhibit maximum elastic strains much lower than their capabilities in free standing state [9, 10]. This obstacle has defied all the efforts to create high-performance metallic composites using nanowires.

It was not until very recently that this challenge is overcome, in an in-situ metallic composite composed of a phase-transforming TiNi matrix and aligned Nb nanowires. In this composite the embedded Nb nanowires are measured to exhibit an elastic lattice strain of over 6% [11], which is several times larger than those reported of namowires in matrices which deform by plasticity via dislocation slip at beyond the elastic limit. The achievement of the ultrahigh elastic strain, thus ultrahigh strength, of the Nb nanowires in this composite is attributed to the strain matching effect between the TiNi matrix and the Nb nanwires [11]. In this case, the uniform lattice strain of the B2-B19' martensitic transformation of the TiNi matrix, typically 6~8%, matches well in magnitude [11-13] with the uniform elastic strain of the Nb nanowires, approximately 6% [14, 15].

The B2-B19' martesitic transformation in NiTi is a first order phase transformation. It occurs discretely at the atomic scale. This imposes a discrete local strain field at the site of the transformation, between a small elastic strain of <1% in the parent phase region and a lattice strain of up to 8% in the martensite region [13, 16]. In addition, this discontinuous strain field at the site of transformation is subjected to the constraint of the uniform elastic strain of the Nb nanowires [11]. This raises questions how the Nb nanowires may respond to the discrete lattice strains of the transforming NiTi matrix with their uniform elastic strains. This study investigates the strain matching behavior between the Nb nanowires and the NiTi matrix by means of synchrotron X-ray diffraction during progressive tensile straining of a TiNi-Nb composite.

Experimental Procedure

A composite ingot with a nominal composition of $Ti_{42}Ni_{38}Nb_{20}$ was prepared by means of vacuum induction melting. The ingot was hot forged at 1123 K and hot drawn into a wire of 0.9 mm in diameter. The wire was annealed at 1023 K for 1.2 ks and then further cold drawn to 0.5 mm in diameter. Test samples of 20 mm in length were cut from the wire and then annealed in air at 748 K for 1.2 ks. In-situ high-energy x-ray diffraction measurements during tensile deformation were performed at room temperature at the 11-ID-C beamline of the advanced photon source, Argonne National Laboratory. Tensile deformation was conducted at a strain rate of 1×10^{-4} s^{-1}. The high-energy x-ray used had a beam spot size of 0.4 mm and a wavelength of 0.10798 Å. Two-dimensional (2D) full circle diffraction patterns were recorded in transmission geometry. One-dimensional (1D) diffraction spectra were generated by integrating the corresponding diffraction intensities within the circular angle ranging from 85° to 95° on 2D diffraction patterns, for which 0° is defined as the transverse direction and is perpendicular to the wire and loading direction. Samples used for TEM study were firstly mechanically grinded to ~40 μm in thickness, followed by ion polishing to below 100 nm. TEM observation was carried out using an FEI Tecnai G20 transmission electron microscope operating at an accelerating voltage of 200 kV.

Results and Discussion

Fig. 1 presents the structural information of the composite wire. Fig. 1A is a TEM bright field image of the longitudinal view. The matrix is polycrystalline NiTi with grain sizes ranging from 20 to 50 nanometers. The Nb nanowires are long and about 50 nanometers in diameter. They are uniformly distributed in the NiTi matrix and are all parallel-aligned along axial direction of the composite wire. Fig. 1B is a synchrotron 2D X-ray diffraction pattern taken with the X-ray beam perpendicular to the wire length. The length direction (LD) and transverse direction (TD) of the wire are marked in the figure. The pattern is fully indexed to the B2-NiTi phase and the body-centered cubic Nb phase. It is evident that the intensity of the $(110)_{Nb}$ diffraction ring is highly concentrated at several spots whereas the intensity of the $(110)_{B2\text{-}NiTi}$ ring is relatively uniform. This indicates the strong wire texture of the Nb nanowires resulting from the wire drawing process, with (110) planes preferentially oriented perpendicular to the axial direction of the composite wire.

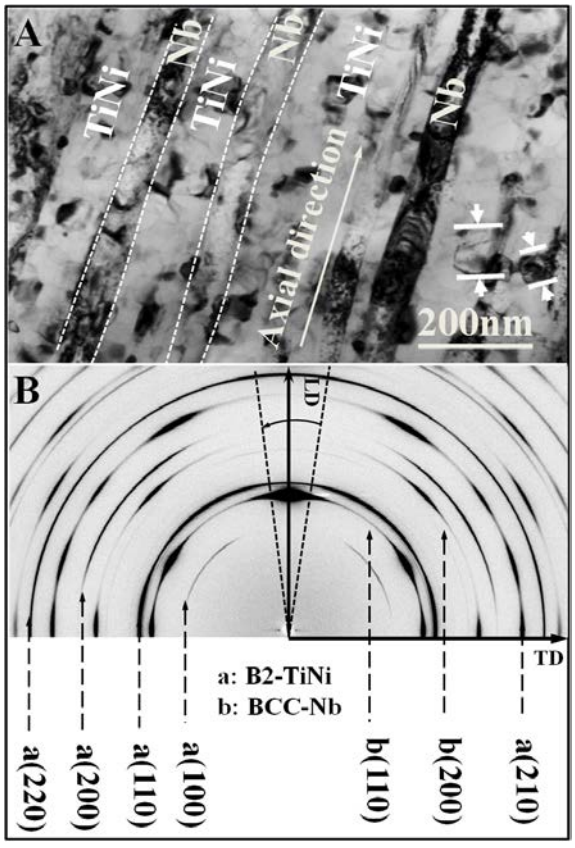

Fig. 1. Microstructure of the TiNi-Nb in-situ composite wire. A. TEM bright field image of the longitudinal view of the wire. B. Synchrotron X-ray 2D diffraction pattern.

Fig. 2 shows the tensile deformation behavior and the corresponding structural evolution of the composite wire. Fig. 2A is the global stress-strain curve of a sample in three tensile deformation cycles. The macroscopic strain recovered upon unloading

during each cycle was more than 6%, indicating that the TiNi matrix of the composite wire has undergone stress induced martensitic (SIM) transformation and recovered. Fig. 2B shows two 1D x-ray diffraction patterns in the axial direction of the sample taken at zero applied strain and 8% applied strain. It is seen that the B2-NiTi diffraction peaks at zero applied strain were replaced by B19'-NiTi peaks at 8% strain, meanwhile the d-spacing of $(110)_{Nb}$ planes obviously increased. The lattice strain of $(110)_{Nb}$ is calculated as $\varepsilon_{(110)}=(d^{(110)}-d_0^{(110)})/d_0$, in which $d^{(110)}$ is the d-spacing of $(110)_{Nb}$ at a given applied strain and $d_0^{(110)}$ is the corresponding lattice spacing at zero strain state. It is evident that at 8% applied strain, the B2-NiTi matrix was completely transformed to the B19' phase, and the embedded nanowires were about 4.6% elastically strained along the loading direction.

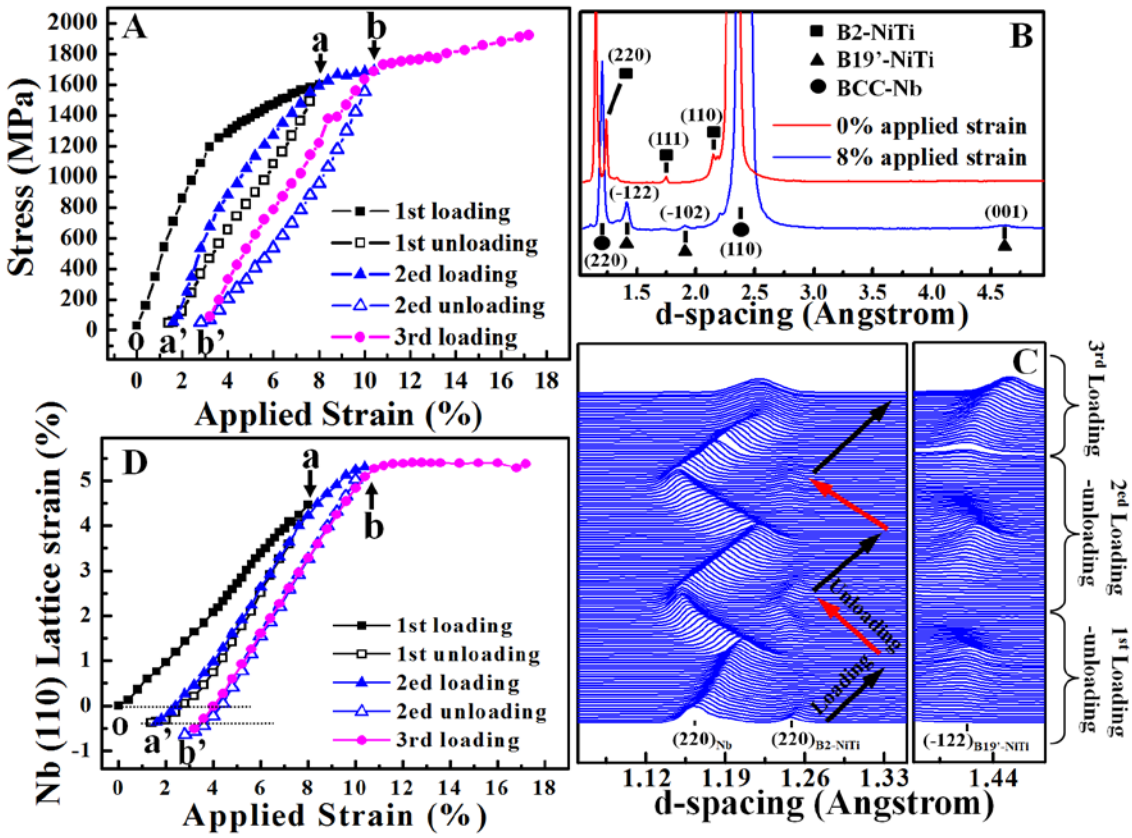

Fig. 2. Tensile deformation behavior of the NiTi-Nb composite. A. Macroscopic tensile stress-strain behavior of the composite wire. B. 1D diffraction spectra of the sample at 0% applied strain and 8% applied strain. C. In-situ X-ray diffraction spectra of the comspoite wire revealing evolution of $(220)_{Nb}$, $(220)_{B2\text{-}NiTi}$ and $(-122)_{B19'\text{-}NiTi}$ peaks during cyclic tensile deformation. D. Evolution of $(110)_{Nb}$ lattic strain as a function of applied strain.

Fig. 2C shows a collection of 1D XRD spectra. They are plotted at every 0.4% of the applied strain. The XRD spectra reveal the evolution of the $(220)_{Nb}$, $(220)_{B2\text{-}NiTi}$ and $(-122)_{B19'\text{-}NiTi}$ peaks during the three deformation cycles. It is seen that the $(220)_{B2\text{-}NiTi}$ and $(-122)_{B19'\text{-}NiTi}$ peaks gradually diminished upon loading and then emerged upon

unloading in turn. Accompanying this, the $(220)_{Nb}$ peak shifted gradually to higher d-spacing values upon loading and returned to lower d-spacing values after unloading. This indicates that the NiTi matrix experienced reversible stress-induced B2↔B19' martensitic transformations while the embedded Nb nanowires stretched and recovered elastically during the deformation cycles.

Fig. 2D shows the evolution of the elastic (220) lattice strain of the Nb nanowires during the tensile cycles. It is of interest to note that after the first tensile cycle, the Nb lattice strain was negative (point a'), indicating a compressive strain in the axial direction after one deformation cycle. It is also evident that the compressive strain increased after the second tensile cycle (point b'). The compressive lattice strain after the deformation cycle implies that plastic deformation has occurred in the Nb nanowires during the deformation cycle, although the $(220)_{Nb}$ lattice strain vs. applied strain kept linear relationship and the maximum strain of $(220)_{Nb}$ was 4.5% in the first deformation cycle, being smaller than the elastic strain limit of the Nb nanowires, which was about 5.5% in this composite.

The occurrence of plastic deformation in the Nb nanwires is attributed to the discrete nature of the martensitic transformation of the NiTi matrix. This is schematically shown in Fig. 3. The B2-B19' martensitic transformation in NiTi is a first order transformation and it occurs discretely at the atomic level with lattice distortions ranging between 4 and 8% shear strain [16, 17]. Macroscopically the SIM may occur either in a uniform manner or a Lüders type manner [12, 18, 19]. In this study, the stress induced B2→B19' transformation in the matrix occurred in a macroscopically uniform manner, as evidenced in Fig. 2A (the absence of an obvious Lüders type stress plateau on the stress-strain curve). That means, even at relatively small global strain levels for the composite wire, the B2→B19' martensitic transformation occurs in the matrix uniformly in a mosaic-like manner, as schematically shown in Fig. 3B. Increasing the global strain of the composite wire leads to the increas in the volume fraction of the transformed B19' phase in the NiTi matrix and increase of the elastic strain in the Nb nanowires, as schematically shown in Fig. 3D.

Fig. 3C shows a local scene of a Nb nanowire and its adjacent NiTi matrix, part of which has transformed to B19' martensite. The strain distributions along lines a and b are shown on the right, for a nominal condition of 3% global strain. Ignoring the coupling effect, or the constraint, between the NiTi matrix and the Nb nanowire, the NiTi matrix exhibits discrete steps corresponding to the elastic strain of the B2 phase and the lattice distortion strain of the B19' phase whereas the Nb nanowire experiences a uniform 3% elastic strain along its length. Line c indicates the elastic strain limit of the Nb nanowire. However, under the constraint of the surrounding matrix, the strain distribution along line b is modified to b', which indicates that the section of a Nb nanowire adjacent to B19' phase of the matrix is subjected to a tensile strain greater than its elastic strain limit, implying the occurrence of local plastic deformation. The condition after unloading is shown in Fig. 3E, where the NiTi

matrix has fully recovered both structurally back to the B2 phase and mechanically to its original dimension and the embedded Nb nanowires have recovered their elastic strains but retained some local plastic strains. Fig. 3F shows a local scene. The shaded sections of the Nb nanowire indicate the plastically deformed sections. The strain distributions along lines a and b are shown on the right. It is seen that the sections of the Nb nanowires that have been plastically deformed are subjected to compressive strains.

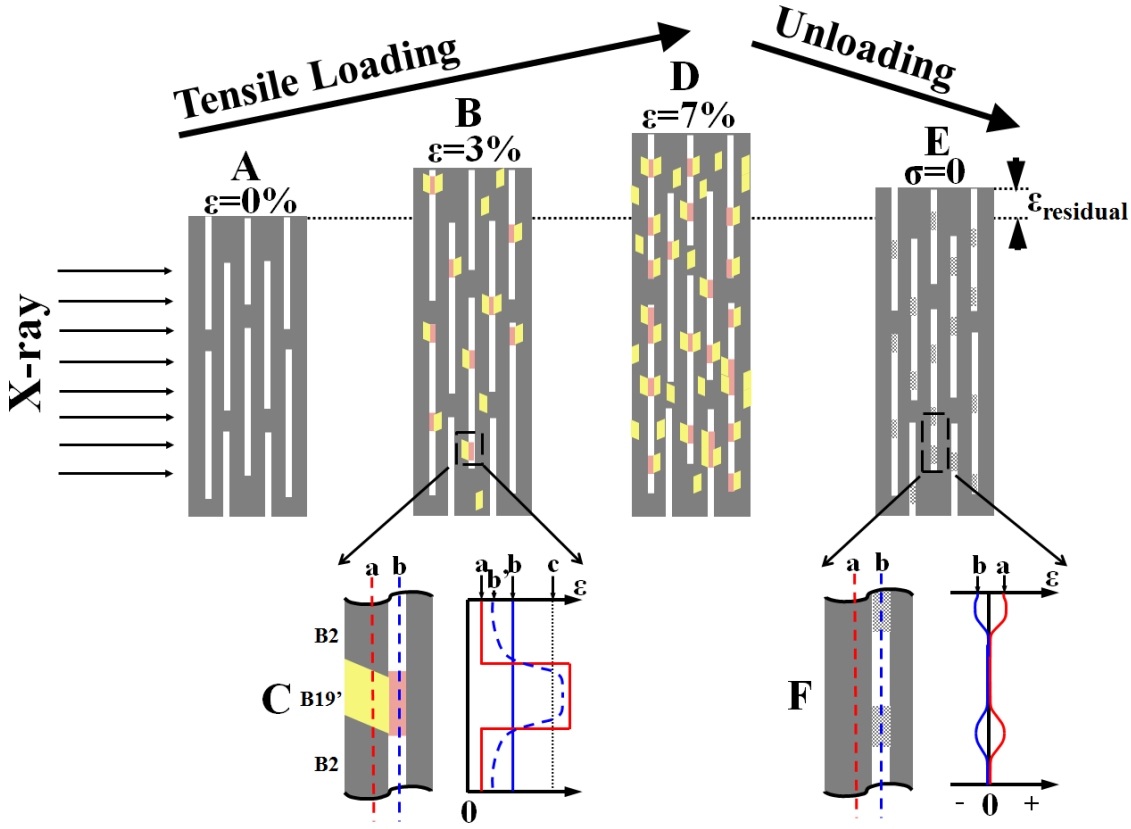

Fig. 3. Schematic illustration of the deformation mechanism of the elastic Nb nanowires and the NiTi transforming matrix in a composite wire in tension.

The above discussion demonstrates clearly that plastic deformation may occur in embedded nanowires in a phase transforming matrix even at global strains well below the expected elastic strain limit of the nanowires. This finding clarifies that, the plastic deformation of nanowire was determined by the SIM of surrounding NiTi matrix rather than the magnitude of applied strain on the composite. It rectifies an earlier recommendation that the composite wire needs to be deformed to well beyond the elastic strain limit of the embedded nanowires in order to introduce plastic strains in the nanowires, to achieve strain coupling between the two components for desired global mechanical properties [11].

Conclusion

In the phase transformation matrix-nanowire composite system, plastic deformation may occur in the embedded nanowires at global strains well below the expected elastic strain limit of the nanowires. This is attributed to the discrete nature of the first order phase transformation of the matrix and the strain coupling effect between the two components. The occurrence of the internal plastic deformation of the nanowires provides an opportunity for tailoring internal residual stresses for property control of the composite.

Acknowledgements:

This work is supported by the key program project of National Natural Science Foundation of China (NSFC) (51231008), Australian Research Council (Grant No. DP140103805), the National 973 programs of China (2012CB619400), National Natural Science Foundation of China (NSFC) (51101170), Key Project of Chinese Ministry of Education (313055). Use of the Advanced Photon Source was supported by the U.S. Department of Energy, Office of Science, Office of Basic Energy Sciences, under Contract No. DE-AC02-06CH11357

References

[1] K. Koziol, J. Vilatela, A. Moisala, M. Motta, P. Cunniff, M. Sennett, A. Windle, Science, 318 (2007) 1892-1895.

[2] T. Zhu, J. Li, Prog. Mater Sci. , 55 (2010) 710-757.

[3] S. Ying, S. Jianren, L. Miao, C. Quanfang, Nanotechnology, 18 (2007) 505704.

[4] E. Neubauer, M. Kitzmantel, M. Hulman, P. Angerer, Composites Science and Technology, 70 (2010) 2228-2236.

[5] Y.B. Tang, Y.Q. Liu, C.H. Sun, H.T. Cong, J. Mater. Res. , 22 (2007) 2711-2718.

[6] L. Thilly, P.O. Renault, V. Vidal, F. Lecouturier, S. Van Petegem, U. Stuhr, H. Van Swygenhoven, Appl. Phys. Lett. , 88 (2006) 191906.

[7] V. Vidal, L. Thilly, S. Vanpetegem, U. Stuhr, F. Lecouturier, P. Renault, H. Vanswygenhoven, Scr. Mater. , 60 (2009) 171-174.

[8] K. Han, J.D. Embury, J.R. Sims, L.J. Campbell, H.J. Schneider-Muntau, V.I. Pantsyrnyi, A. Shikov, A. Nikulin, A. Vorobieva, Mater. Sci. Eng., A, 267 (1999) 99-114.

[9] J.-B. Dubois, L. Thilly, P.-O. Renault, F. Lecouturier, Adv. Eng. Mater. , 14 (2012) 998-1003.

[10] L. Thilly, S.V. Petegem, P.-O. Renault, F. Lecouturier, V. Vidal, B. Schmitt, H.V. Swygenhoven, Acta Mater. , 57 (2009) 3157-3169.

[11] S. Hao, L. Cui, D. Jiang, X. Han, Y. Ren, J. Jiang, Y. Liu, Z. Liu, S. Mao, Y. Wang, Y. Li, X. Ren, X. Ding, S. Wang, C. Yu, X. Shi, M. Du, F. Yang, Y. Zheng, Z. Zhang, X. Li, D.E. Brown, J. Li, Science, 339 (2013) 1191-1194.

[12] P. Sittner, Y. Liu, V. Novak, Journal of the Mechanics and Physics of Solids, 53 (2005) 1719-1746.

[13] K. Otsuka, X. Ren, Prog. Mater Sci. , 50 (2005) 511-678.

[14] Y. Yue, P. Liu, Z. Zhang, X. Han, E. Ma, Nano Lett. , 11 (2011) 3151-3155.

[15] B. Wu, A. Heidelberg, J.J. Boland, Nat. Mater. , 4 (2005) 525-529.

[16] X. Zhang, H. Sehitoglu, Mater. Sci. Eng., A 374 (2004) 292-302.

[17] S. Miyazaki, K. Otsuka, Y. Suzuki, Scripta Metallurgica, 15 (1981) 287-292.

[18] Y. Liu, Y. Liu, J. Humbeeck, Scr. Mater. , 39 (1998) 1047-1055.

[19] G. Tan, Y. Liu, P. Sittner, M. Saunders, Scr. Mater. , 50 (2004) 193-198.